NANO LETTERS

pubs.acs.org/NanoLett Letter

Amorphous Thickness-Dependent Strengthening−Softening Transition in Crystalline−Amorphous Nanocomposites

Lei Qian, Wenqing Yang, Jiasi Luo, Yunjiang Wang, K. C. Chan, and Xu-Sheng Yang*

Cite This: https://doi.org/10.1021/acs.nanolett.3c03848 Read Online

ACCESS | Metrics & More | Article Recommendations | Supporting Information

ABSTRACT: Core−shell crystalline−amorphous nanocomposites, featuring nanograins surrounded by thick amorphous boundaries, are promising nanoarchitectures for achieving exceptional strength through cooperative strengthening effects. However, a comprehensive understanding of the influence of characteristic sizes, particularly the amorphous thickness, on codeformation strengthening is still lacking, limiting the attainment of the strength limit. Here, we employ molecular dynamics simulations to investigate Cu-CuTa crystalline−amorphous nanocomposites with varying grain sizes and amorphous thicknesses. Our findings demonstrate significant strengthening effects in nanocomposites, effectively suppressing the Hall−Petch breakdown observed in traditional amorphous-free nanograined Cu. Intriguingly, we observe a maximum strength followed by a strengthening−softening transition dependent on the amorphous thickness, as exemplified by a representative nanocomposite featuring a 12.5 nm grain size and a critical amorphous thickness of 4 nm. Inspired by observed shifts in atomistic mechanisms, we developed a theoretical model encompassing variations in grain size and amorphous thickness, providing valuable insights into the size−strength relationship for crystalline−amorphous nanocomposites.

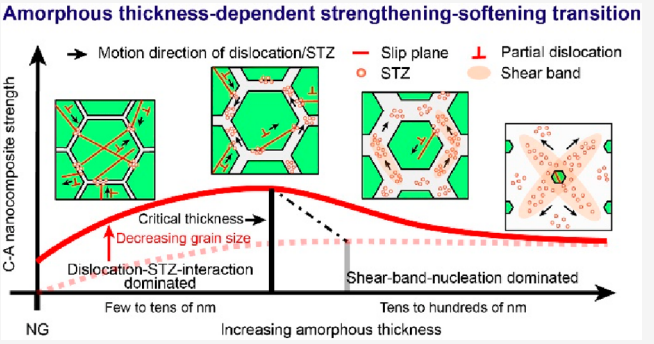

KEYWORDS: *crystalline−amorphous nanocomposite, Cu-CuTa, atomistic simulations, codeformation cooperative mechanisms*

The pursuit of ultrahigh strength in metals has driven significant advancements in metal design. Nanostructuring stands out as a prominent strategy, extensively applied to explore strength limits in both crystalline and amorphous metals.[1−4] Nanocrystalline (NC) metals, characterized by refined grain size and increased grain boundary (GB) density, leverage the Hall−Petch strengthening,[5,6] where GBs resist dislocation motion. However, NC metals with extremely small grain sizes can experience a strengthening−softening transition, known as the Hall−Petch breakdown, where GB-mediated plasticity dominates over GB strengthening.[7−9]

Concurrently, nanosized amorphous metals exhibit an enhanced ability to suppress localized shear bands, thereby contributing to an ideal strength with enhanced ductility.[1,10] Building upon the success of introducing structural heterogeneity to improve strength,[11−15] a new strategy has emerged that combines the structural advantages of crystalline and amorphous nanostructures in a complementary manner. This strategy has led to the development of crystalline−amorphous nanocomposites,[16−21] where nanograins are encapsulated by nanosized thick amorphous GBs. In these nanocomposites, the ultrastrong amorphous GBs effectively impede or absorb dislocation activities within nanograins,[22,23] preserving the Hall−Petch strengthening effect even at extremely refined grain sizes.[16] Additionally, the accommodation of dislocation activities restrains the plastic instability of the nanosized amorphous phase, inhibiting localized shear band propagation and promoting the activation of homogeneous shear transformation zones (STZs).[24,25] Consequently, the distinctive codeformation cooperative strengthening effect in crystalline−amorphous nanocomposites can yield a remarkable strength−ductility synergy,[20,26,27] surpassing the overall strength of the individual constituents.[28,29]

To date, experimental synthesis of crystalline−amorphous nanocomposites has been achieved through various methods, such as GB doping,[26,30−32] laser-related processing,[33,34] and severe plastic deformation[35−37] of the crystalline matrix, showing promise in diverse applications. Experimental investigations have demonstrated improved strength accompanied by significant codeformation capability in these nanocomposites.[18,20,25,38] However, it should be noted that in relatively large-scale amorphous constituents, plasticity is governed by localized shear bands.[39,40] In crystalline−amorphous nanocomposites, the sustained presence of

Received: October 8, 2023
Revised: November 14, 2023
Accepted: November 14, 2023

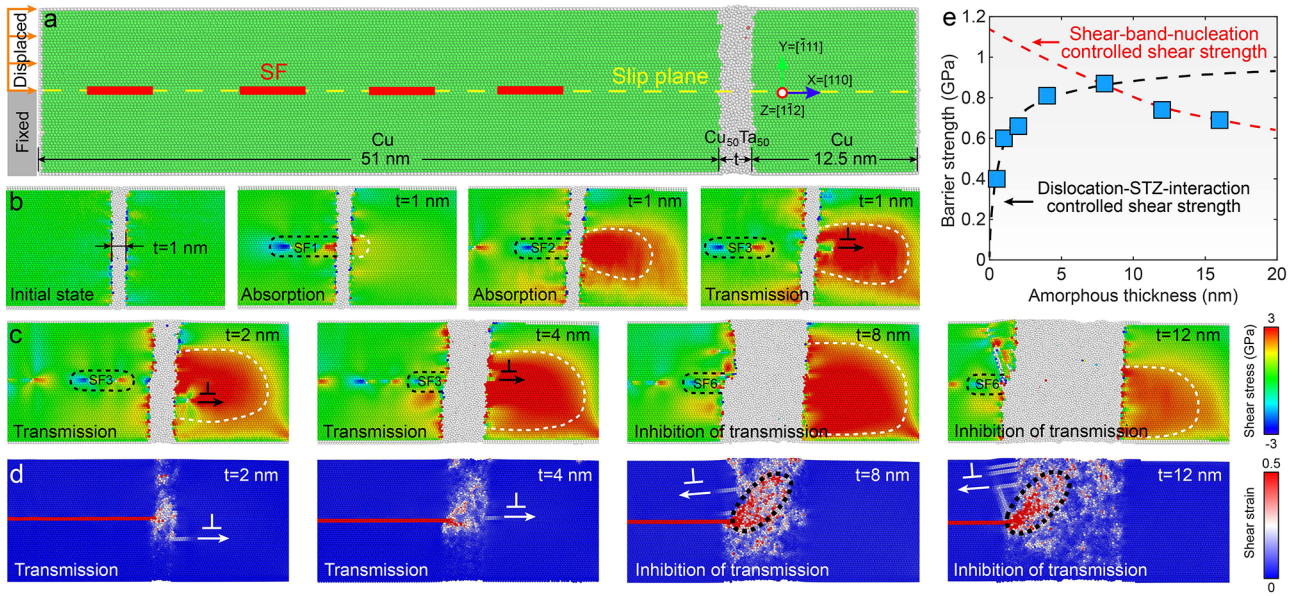

Figure 1. Atomistic simulation of simple crystalline−amorphous nanolayers under shear deformation. (a) Simulation model and computational setup. (b) Evolution of atomic shear stress field for a nanolayer with a 1 nm amorphous thickness. (c) Shear stress distributions of nanolayers after yielding an amorphous layer with varying amorphous thicknesses. In (b) and (c), only atoms inside the crystalline layer are colored according to shear stress magnitudes. (d) Shear strain distributions of nanolayers after yielding of an amorphous layer with varying amorphous thicknesses. (e) Variation of amorphous layer barrier strength with respect to amorphous thickness.

advantageous homogeneous STZs within the amorphous GBs may be compromised if the GB thickness is significantly increased.[29,41,42] In other words, such codeformation cooperative and associated strengthening effects might lose effectiveness, leading to a strengthening−softening transition and a peak strength at a specific grain size, dependent on the amorphous GB thickness. However, the flexible fabrication of crystalline−amorphous nanocomposites with uniform microstructures and varying characteristic sizes remains challenging. Meanwhile, the commonly observed inhomogeneous distribution of amorphous GBs in experimentally prepared crystalline−amorphous nanocomposites can impede the realization of ideal codeformation, thereby affecting the strengthening effect.[16] These experimental limitations constrain our comprehensive understanding of the influence of characteristic sizes, especially the amorphous thickness, on codeformation strengthening and achieving the strength limit.

Alternatively, atomistic simulation techniques provide precise control over microstructure and offer insights into the underlying mechanistic rationale,[43−45] deepening our understanding of crystalline−amorphous nanocomposites. Here, we employed MD simulations to construct a series of crystalline−amorphous Cu-CuTa nanocomposites with varying grain sizes and amorphous thicknesses and carried out tensile tests. Our results demonstrate significant strengthening effects in these nanocomposites, resisting the Hall−Petch breakdown observed in amorphous-free nanograined Cu with an extremely small grain size. Notably, we observe a strength limit, followed by a strengthening−softening transition dependent on the amorphous thickness. This behavior is exemplified by a representative nanocomposite featuring a 12.5 nm grain size and a critical amorphous thickness of 4 nm. Additionally, we investigate the shift of the atomistic plastic mechanisms and develop a theoretical model encompassing variations in grain size and amorphous thickness to elucidate the size−strength relation in crystalline−amorphous Cu-CuTa nanocomposites.

For initial validation, we employed the MD simulations to test the shear deformation of simple crystalline (Cu)−amorphous (CuTa) nanolayers with amorphous thicknesses of t = 0.5−16 nm (details in the Supporting Information). A sequence of stacking faults (SFs) containing a pair of leading and trailing partial dislocations are artificially created in the crystalline region to interact with these amorphous layers, as shown in Figure 1a,b, including dislocation blockage, absorption, and/or transmission. Figure 1c reveals that the maximum local shear stress concentration in the crystalline region induced by dislocation absorption gradually increases with the amorphous thickness when $t \leq 8$ nm, implying the strengthening effect.[22] Moreover, the STZs indicated by high shear strain (here >0.2) are triggered in the yielded amorphous layer to accommodate the localized shear deformation brought by the dislocation absorption and gliding (Figure 1d). However, these STZs prefer to percolate together with the further increased amorphous thickness (t > 8 nm), in which the nucleation of localized shear bands (as marked by the circled area in Figure 1d) is observed to significantly inhibit the transmission of dislocation. When examining corresponding shear stress−strain curves shown in Figure S1 (see the Supporting Information), a drastic stress drop (black arrow) could be observed at the onset of amorphous layer yield, leading to a peak shear stress which represents the barrier strength of the amorphous layer to dislocation motion. It is found that the variation of barrier strength undergoes an amorphous layer thickness-related increasing−decreasing transition with a critical thickness of 8 nm and peak value of ∼0.87 GPa, as shown in Figure 1e, suggesting a strengthening−softening transition. We anticipate that similar behavior would occur in three-dimensional core−shell crystalline−amorphous nanocomposites. Due to the more complex configurations, the transition features (e.g., critical amorphous thickness and peak strength value), underlying atomistic plastic mechanisms and associated theoretical modeling of the crystalline−amorphous

https://doi.org/10.1021/acs.nanolett.3c03848
Nano Lett. XXXX, XXX, XXX−XXX

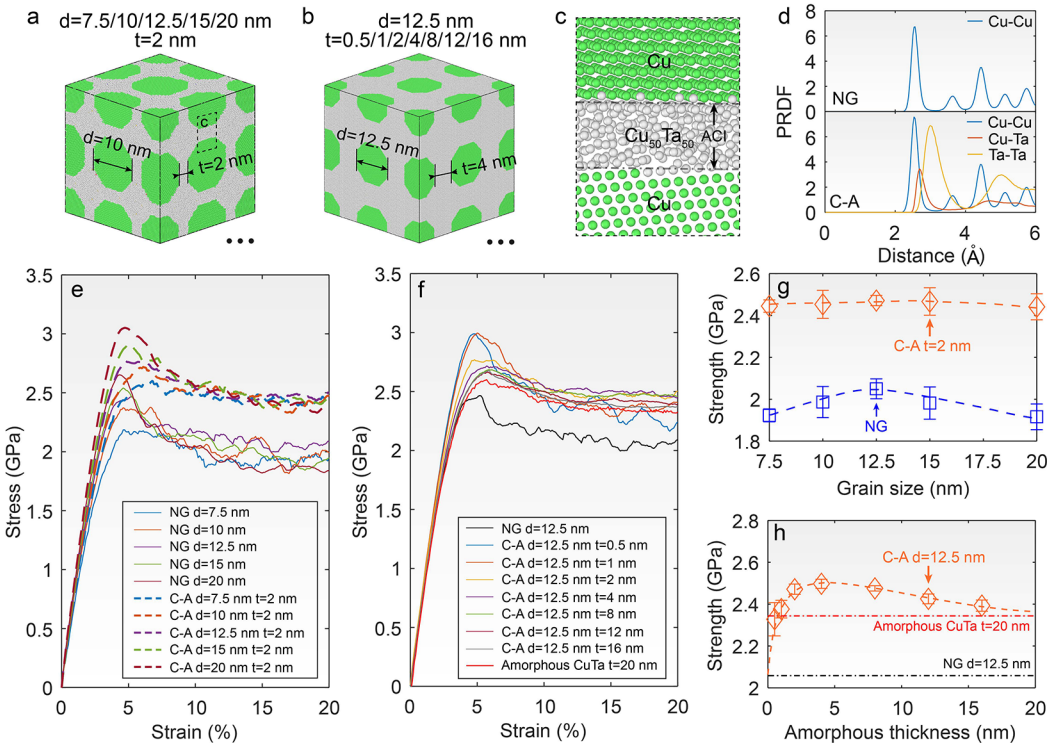

Figure 2. Simulation models and strength performance of core−shell crystalline−amorphous nanocomposites. (a) C-A samples with a 2 nm amorphous shell but different grain sizes. (b) C-A samples with 12.5 nm grain size but different amorphous thicknesses. (c) Magnified view of the crystalline−amorphous nanostructure. (d) Partial radial distribution functions (PRDF) for NG and C-A samples. (e) Stress−strain curves for NG samples and corresponding C-A counterparts with an amorphous thickness of 2 nm. (f) Stress−strain curves for C-A samples having 12.5 nm grain size and varying amorphous thicknesses. (g) Tensile strength as a function of grain size for NG and C-A samples, respectively. (h) Relation of strength vs amorphous thickness for C-A samples. In (g) and (h), the strength of each sample is calculated as the average stress over the strain range of 10−20%.

nanocomposite still need to be explored and understood in depth.

Herein, we constructed two sets of idealized core−shell crystalline−amorphous nanocomposites consisting of randomly distributed nanograined Cu cores surrounded by uniform nanosized amorphous CuTa shells (see the Supporting Information), as shown in Figure 2a,b. A representative atomistic interfacial configuration in Figure 2c and the corresponding partial radial distribution function (PRDF) in Figure 2d verify the core−shell crystalline (Cu)−amorphous (CuTa) nanocomposite structure.[46] Based on the stress−strain curves plotted in Figure 2e, the variations of strength with grain sizes in Figure 2g show that the amorphous-free nanograined (NG) Cu samples have the Hall−Petch breakdown with a maximum strength of ∼2.05 GPa at a critical grain size of ∼12.5 nm, in agreement with previous reports.[47] When fixed 2 nm thick amorphous GBs are implanted into these NG samples, the resultant core−shell counterparts exhibit a significantly increased strength to ∼2.45 GPa and no obvious Hall−Petch breakdown. We deliberately chose the nanocomposite with the strongest grain size (d = 12.5 nm) to investigate the influence of varying the amorphous thickness on its strength performance. This selection is motivated by our interest in understanding the strength limits within the crystalline−amorphous nanocomposite being studied. As shown in Figure 2f,h, the nanocomposites with a fixed grain size of 12.5 nm but different amorphous grain boundary thicknesses exhibit a noticeable overall strengthening effect, surpassing that of amorphous CuTa. Specifically, as the amorphous thickness increases, the strength initially rises to a peak value of approximately 2.5 GPa at t = 4 nm and then gradually decreases toward the strength observed in purely amorphous CuTa. This behavior demonstrates a transition from strengthening to softening with increasing amorphous thickness.

Figure 3 provides atomic images to illustrate the underlying plastic deformation (especially the strengthening−softening transition) mechanisms of the above nanocomposites with a fixed 12.5 nm grain size but varying amorphous GB thicknesses. The snapshots at a strain of 10% in Figure 3a show that the deformation of the crystalline core can be ascribed to dislocation activities for all simulated nanocomposites, mainly in the form of partial dislocations indicated by green lines. The structural evolution of a representative nanocomposite with t = 4 nm (Figure 3b) demonstrates that partial dislocations preferentially nucleate from the amorphous−crystalline interfaces (ACIs) and then propagate across the nanograins with the progress of straining, followed by the formation of SFs. It is further found from the magnified view that dislocations would trigger the activation of STZs inside the amorphous shell when arriving at ACIs, implying a dislocation−STZ interaction-based cooperative codeformation. Note that such a codeformation action could have an obvious strengthening effect and facilitate reallocating the stress and strain.[23,48] Figure 3c presents the evolution of the dislocation density within the crystalline core of simulated nanocomposites. This dynamic dislocation density is governed by the interplay among dislocation generation, glide, and

https://doi.org/10.1021/acs.nanolett.3c03848
Nano Lett. XXXX, XXX, XXX−XXX

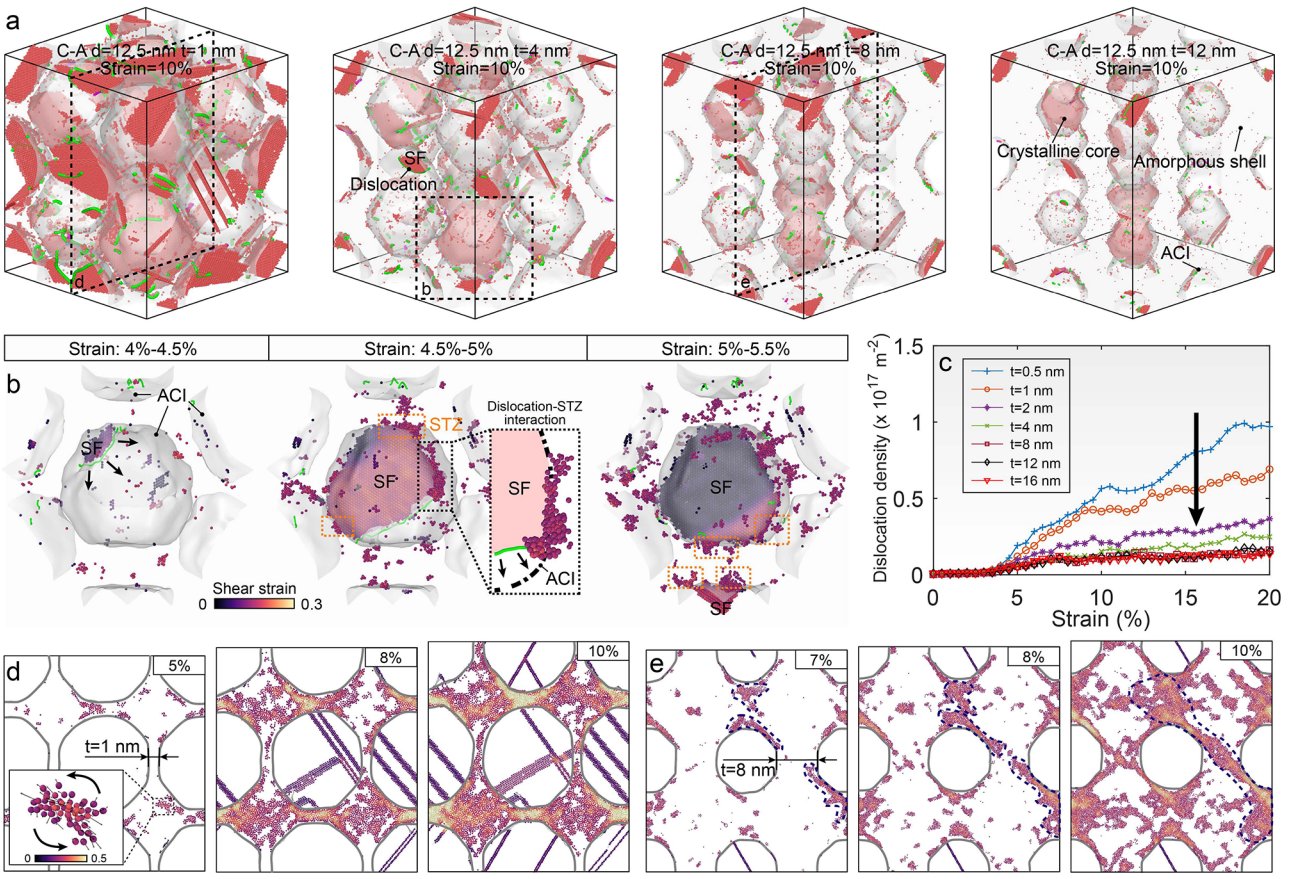

Figure 3. Underlying deformation mechanisms in core−shell crystalline−amorphous nanocomposites. (a) Dislocation structures in C-A nanocomposites with various amorphous thicknesses at 10% strain. For better visualization, only slip atoms (red) and reconstructed ACIs are shown. (b) Structural evolution of a representative nanograin inside a nanocomposite with t = 4 nm, revealing the interaction between dislocation and STZ during straining. Newly activated STZs are observed to locate near the intersection between the slip plane and ACI. (c) Evolutions of dislocation density inside a crystalline core with strain for simulated C-A samples. (d, e) Cross-section snapshots of shear strain distribution, showing dislocation slips and accumulated STZs in corresponding samples in (a). In (b), (d), and (e), only disordered atoms with large shear strain (>0.15) and slip atoms are shown and colored according to calculated atomic shear strains.

annihilation during deformation. Importantly, a consistent trend is observed across different amorphous thicknesses: at a given strain level, the dislocation density within the crystalline core gradually decreases as the amorphous thickness increases, which is also evidenced in Figure 3a. The observation implies that the probability of dislocation−STZ interaction and associated strengthening effect are anticipated to gradually decline with increasing amorphous thickness.

To further elucidate the responsible mechanisms, both dislocation structures and activated STZs in representative samples with t = 1 and 8 nm are examined at different strain levels, as shown in Figure 3d,e, respectively. For the sample with t = 1 nm illustrated in Figure 3d, a few STZs where atomic rearrangements present circular displacements[49] are first activated near ACIs at the beginning of plastic deformation (~5% strain). When increasing the strain to 8% and 10%, the sustained dislocation activities, such as propagation, blockage, and absorption near ACIs, significantly promote the sites to trigger the STZs that are observed to homogeneously distribute throughout the amorphous GBs. Conversely, fewer dislocation activities are found in the sample with the thicker t = 8 nm, as shown in Figure 3e, which would limit the dislocation−STZ interaction-induced stress and strain allocations. As the strain increases, the activated STZs are observed to gradually percolate along a plane of maximum shear stress and finally aggregate into localized narrow shear bands, as marked by dashed lines in Figure 3e. It would cause the shear band nucleation and thus induce the yielding of the nanocomposite. Therefore, the dominant mechanisms from dislocation−STZ interaction codeformation to shear band nucleation should be responsible for the strengthening−softening transition with a critical thickness of 4 nm at a given grain size of 12.5 nm, as the strength evolution shown in Figure 2h.

The strength of a crystalline−amorphous nanocomposite can be theoretically described according to the rule of mixture (ROM) combining the weighted strength of individual parts,[41] which is expressed as

$$\sigma_{C\text{-}A} = V_C\sigma_C + V_A\sigma_A \tag{1}$$

$$V_C = \left(\frac{d}{d+t}\right)^3 \quad V_A = 1 - \left(\frac{d}{d+t}\right)^3 \tag{2}$$

where V and σ represent the volume fraction and theoretical strength of individual parts which both depend on their intrinsic sizes and C and A refer to the crystalline and amorphous parts, respectively. By assuming the nanograin has a uniform shape of a sphere and treating grain size d and amorphous thickness t as the key microstructural parameters,

https://doi.org/10.1021/acs.nanolett.3c03848
Nano Lett. XXXX, XXX, XXX−XXX

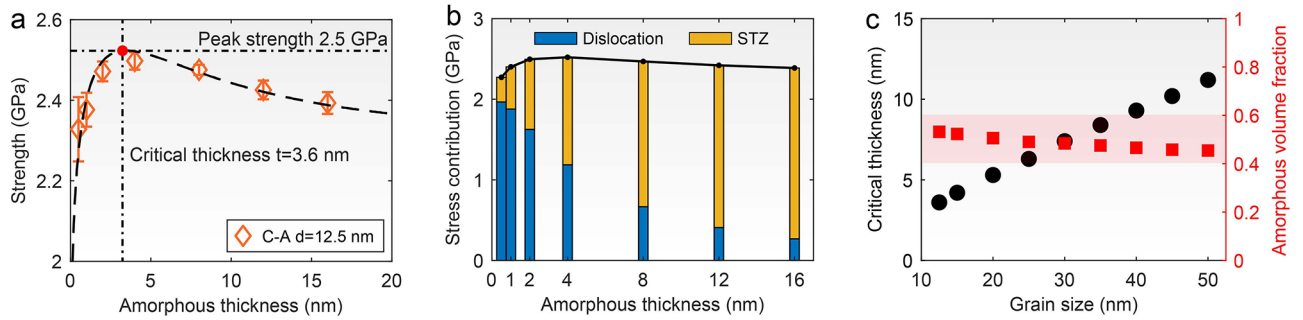

Figure 4. Amorphous thickness-dependent strengths of core−shell crystalline−amorphous nanocomposites. (a) Comparison of the predictions by using eq 6 with simulation results for variation of strength with amorphous thickness. (b) Calculated stress contribution evolution from dislocations activities and STZ-related processes with amorphous thickness in crystalline−amorphous nanocomposties with a grain size of 12.5 nm. (c) Predicted critical amorphous thicknesses and corresponding amorphous volume fractions in nanocomposites with different grain sizes.

the volume fractions of individual phases could be simply calculated as shown in eq 2.

Given that the strengthening effect can be sustained for the extremely refined nanograins in crystalline−amorphous nanocomposites, as shown in Figure 2g, the associated grain-size-dependent strengthening for the crystalline part in the nanocomposites could be expressed by the classical empirical Hall−Petch relation[6]

$$\sigma_C = \sigma_0 + \frac{k}{\sqrt{d}} \tag{3}$$

where σ_0 is the friction stress and its magnitude σ_0 = 0.8 GPa could be determined by the fitting line intercept of amorphous-free NG Cu strengths with varying grain sizes. k is the coefficient characterizing the GB barrier to slip transmission of dislocation and signifies the strengthening effect of different GB types on nanograins, which could be described by $k_{shear} = \sqrt{\frac{\tau\mu b}{\pi(1-\upsilon)}}$ under shear deformation.[22,50] In this equation, τ is the critical shear stress required for slip transmission of dislocation across GBs, representing the boundary barrier strength, μ is the shear modulus, b is the magnitude of the Burgers vector, and υ is the Poisson ratio. Based on the Hall−Petch equation, the strengthening effect becomes more prominent when increasing the k value. Noticeably, our simulation results reveal that amorphous-state CuTa GBs present an enhanced dislocation barrier and strengthening effect, as in the power-law relation plotted in Figure 1e. On this basis, the thicker amorphous layer theoretically contributes to a greater k. Substituting material parameters μ = 48 GPa, b = 0.25 nm, and υ = 0.3 for Cu and the calculated barrier strengths for varying amorphous thicknesses (0.5−8 nm) given in Figure 1e into the equation $k_{shear} = \sqrt{\frac{\tau\mu b}{\pi(1-\upsilon)}}$, we obtain a series of k_{shear} values with the amorphous GB thicknesses, which follows a power-law relation as $k_{shear} = 1.71\left(\frac{t}{t_0}\right)^{0.14}$ GPa nm$^{1/2}$ with a good fitting (see Figure S3 in the Supporting Information). Hence, we propose the simple relation of $k = \alpha\left(\frac{t}{t_0}\right)^{\beta}$ to depict this dependence, where α and β are material-related parameters. β is set to be a constant, and t_0 is added into the equation as a reference thickness with the same unit as t, thereby ensuring that the k and α have the same unit of GPa nm$^{1/2}$. Accordingly, the modified Hall−Petch model involving both the grain size and amorphous thickness is used to represent the strengthening effect of the crystalline part as follows:

$$\sigma_C = \sigma_0 + \frac{\alpha\left(\frac{t}{t_0}\right)^{\beta}}{\sqrt{d}} \tag{4}$$

It was reported that the shear banding becomes a nucleation-controlled event via the activation of STZs when the sizes of bulk metallic glass or amorphous metals decrease into the nanometer regime.[1,39] For example, a theoretical description with the shifted $D^{-0.5}$ power-law dependence was proposed to estimate the shear band nucleation-controlled strength of the metallic glass nanopillars with decreasing diameter of D.[51,52] Figure 4 has demonstrated that the codeformation mode with dislocation−STZ interaction gradually transits to shear band nucleation with amorphous thickness in the nanocomposite, resulting in a softening effect. A similar relation is therefore proposed to express the strength of amorphous shell as

$$\sigma_A = \sqrt{{\sigma_{bulk}}^2 + \frac{\psi}{t}} \tag{5}$$

where σ_{bulk} is the strength of corresponding bulk amorphous metal taken as a simulated strength of ∼2.3 GPa for purely amorphous CuTa with t = 20 nm. ψ is the constant for a particular amorphous material. Combining eqs 1−5, the theoretical model gets refined to

$$\sigma_{C\text{-}A} = \left(\frac{d}{d+t}\right)^3\left(\sigma_0 + \frac{\alpha\left(\frac{t}{t_0}\right)^{\beta}}{\sqrt{d}}\right) + \left(1 - \left(\frac{d}{d+t}\right)^3\right)\sqrt{{\sigma_{bulk}}^2 + \frac{\psi}{t}} \tag{6}$$

where the values of α, β, and ψ can be determined by fitting the simulated results. Consequently, eq 6 shows a good fitting of the simulated strengths of the samples with d = 12.5 nm but varying amorphous thicknesses, denoting α = 5.54 GPa nm$^{1/2}$, β = 0.15, and ψ = 1.15, as shown in Figure 4a. α and β with positive values represent an increased dislocation barrier of the thicker amorphous shell. Taking the Taylor factor of 3.1, the coefficient k can be converted as $k_{shear} = \frac{k}{3.1} = 1.79\left(\frac{t}{t_0}\right)^{0.15}$ GPa nm$^{1/2}$, in good agreement

https://doi.org/10.1021/acs.nanolett.3c03848
Nano Lett. XXXX, XXX, XXX−XXX

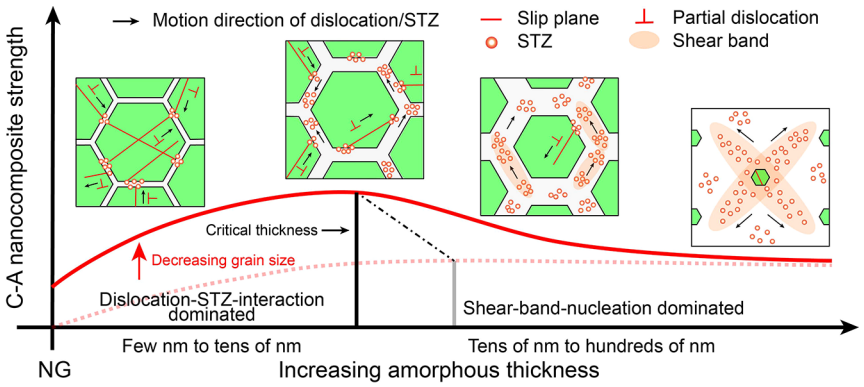

Figure 5. Schematic diagrams of thickness-dependent deformation mechanisms and strengthening effects in core−shell-like crystalline−amorphous nanocomposites.

with the above-fitted relation $k_{shear} = 1.71\left(\frac{t}{t_0}\right)^{0.14}$ GPa nm$^{1/2}$ based on data in Figure 1e. Moreover, the evolution of theoretical strengths of core−shell nanocomposites with amorphous thickness at a series of given grain sizes is plotted in Figure S4 using the developed model (see the Supporting Information). The predicted strengths rationally display a transition from strengthening to softening with different critical values of amorphous thicknesses in nanocomposites.

To clearly category the stress contributions from dislocation activities and STZ-related processes in crystalline−amorphous nanocomposites, eq 6 is modified as

$$\sigma_{C\text{-}A} = \left(\frac{d}{d+t}\right)^3\left(\sigma_0 + \frac{\alpha\left(\frac{t}{t_0}\right)^{\beta}}{\sqrt{d}}\right) + \left(1 - \left(\frac{d}{d+t}\right)^3\right)\sqrt{{\sigma_{bulk}}^2 + \frac{\psi}{t}} = \sigma_{dis} + \sigma_{STZ} \quad (7)$$

Accordingly, Figure 4b illustrates the stress contribution evolution with amorphous thickness in crystalline−amorphous nanocomposites with a grain size of 12.5 nm. The results show that dislocation-related stress accounts for a greater proportion of the overall strength than that of STZs until the critical amorphous thickness of 4 nm is reached. Beyond this critical thickness, the process related to STZs becomes dominant and contributes more to the overall strength. At the critical amorphous thickness of 4 nm, the strength contributions from individual parts are almost equal, indicating a most effective manner in coupling dislocation activities in the crystalline core and STZ processes in the amorphous shell through a dislocation−STZ interaction. It has been demonstrated that the highest strengths of crystalline−amorphous nanocomposites are achieved when both the crystalline and amorphous phases deform homogeneously.[28,29] Additionally, Figure 4c presents the predicted critical amorphous thicknesses for various grain sizes and the corresponding amorphous volume fractions at these critical thicknesses. The results suggest that the critical amorphous thickness, at which the formed crystalline−amorphous nanocomposite achieves its optimal strength, monotonically increases as the grain size increases, resulting in a reasonable amorphous volume fraction within the range of 40−60%. Similar patterns have been observed in experimental studies on CuZr-based crystalline−amorphous nanostructures with different volume fractions of the amorphous phase.[41]

According to previous reports on core−shell crystalline−amorphous nanocomposites,[16,18,22] the remarkable strengthening effect has been understood to stem from the presence of thicker amorphous GBs, seemingly implying a "thicker is stronger" rationale for potential strength enhancement. Nonetheless, the absence of a well-established one-to-one correlation between varying GB thicknesses and the resultant strengths has left the intrinsic size dependence on strength and the deformation mechanism relatively unexplored. Employing MD simulations, we designed and tested a series of crystalline−amorphous Cu-CuTa nanocomposites characterized by varying grain sizes and amorphous thicknesses. This enables us to systematically investigate the thickness-dependent plastic mechanisms responsible for the variations in the overall strength of crystalline−amorphous nanocomposites, thereby establishing a direct correlation between the amorphous thickness and strength. As schematically illustrated in Figure 5, one of the most intriguing findings of this study lies in the observation that the strengthening effect eventually reaches a point of saturation, giving way to a transition toward a softening effect under specific microstructural conditions. Upon replacing the traditional GBs with amorphous-state GBs, the continuous nucleation−propagation−transmission behavior of dislocation plasticity in the NG sample is constrained due to the dislocation blockage/absorption of the amorphous GBs.[6] Initially, the codeformation cooperative mode, achieved through the interaction between constrained dislocation activity and STZ activation, governs the deformation. This codeformation mode, which is well-documented in the literature,[20,26,27] leads to a substantial strengthening effect that positively impacts the strength performance of crystalline−amorphous nanostructures, particularly when amorphous GBs possess only a few nanometers in thickness.[22,23] However, with a further increase in amorphous thickness, the efficacy of the codeformation mode weakens due to the reduced probability of dislocation−STZ interaction. Meanwhile, the intrinsic nature of amorphous structures allows self-activated STZs to percolate within the thick amorphous GB, thereby initiating the localized deformation on a larger scale.[41,42] As a result, plasticity becomes predominantly controlled by the percolation of STZs within the amorphous phase, potentially leading to localized shear band nucleation. Accordingly, the strength of the crystalline−amorphous nanocomposite cannot

https://doi.org/10.1021/acs.nanolett.3c03848
Nano Lett. XXXX, XXX, XXX−XXX

increase indefinitely with increasing amorphous thickness and is expected to return to the level of the nanoscale amorphous CuTa following a softening behavior. This complex interplay culminates in a strength peak and a notable strengthening−softening transition.

It should be also noted that the grain size is another crucial factor influencing codeformation strengthening in crystalline−amorphous nanocomposites, aside from its role in Hall−Petch strengthening.[42] In this study, we mainly focus on the strength variation with amorphous thickness for the strongest NG counterpart, characterized by a 12.5 nm grain size, to push the boundaries of the strength limit. Our developed theoretical model suggests that the observed thickness-dependent strengthening−softening transition can be extended to a wide range of grain sizes, while the critical amorphous thickness necessary for achieving the most homogeneous codeformation is dependent on the grain size. Smaller nanograins in the crystalline−amorphous nanocomposite may require a thinner amorphous shell to reach the optimal microstructural condition for achieving the highest codeformation capacity. Additional simulation works might be warranted in the future to more comprehensively explore the correlation between the critical amorphous thickness and grain size. To summarize, this work successfully establishes a fundamental link between characteristic sizes and deformation mechanisms via a combination of detailed atomistic process observation and theoretical modeling, providing valuable insights into the optimal strength design of crystalline−amorphous nanocomposites.

■ ASSOCIATED CONTENT

Supporting Information

The Supporting Information is available free of charge at https://pubs.acs.org/doi/10.1021/acs.nanolett.3c03848.

Details on materials and methods, including atomistic MD simulations, atomic configuration of simple crystalline−amorphous nanolayer and construction of core−shell crystalline−amorphous nanocomposites, and additional figures, including shear stress evolution, simulation models, fitted power-law relation, and predicted theoretical strengths of crystalline−amorphous nanocomposites (PDF)

■ AUTHOR INFORMATION

Corresponding Author

Xu-Sheng Yang − *Department of Industrial and Systems Engineering, Research Institute for Advanced Manufacturing, The Hong Kong Polytechnic University, Kowloon, Hong Kong 999077, People's Republic of China; Hong Kong Polytechnic University Shenzhen Research Institute, Shenzhen 518060, People's Republic of China;* orcid.org/0000-0003-0769-778X; Email: xsyang@polyu.edu.hk

Authors

Lei Qian − *Department of Industrial and Systems Engineering, Research Institute for Advanced Manufacturing, The Hong Kong Polytechnic University, Kowloon, Hong Kong 999077, People's Republic of China; Hong Kong Polytechnic University Shenzhen Research Institute, Shenzhen 518060, People's Republic of China*

Wenqing Yang − *Department of Industrial and Systems Engineering, Research Institute for Advanced Manufacturing, The Hong Kong Polytechnic University, Kowloon, Hong Kong 999077, People's Republic of China*

Jiasi Luo − *Department of Industrial and Systems Engineering, Research Institute for Advanced Manufacturing, The Hong Kong Polytechnic University, Kowloon, Hong Kong 999077, People's Republic of China*

Yunjiang Wang − *State Key Laboratory of Nonlinear Mechanics, Institute of Mechanics, Chinese Academy of Sciences, Beijing 100080, People's Republic of China;* orcid.org/0000-0002-2969-3889

K. C. Chan − *Department of Industrial and Systems Engineering, Research Institute for Advanced Manufacturing, The Hong Kong Polytechnic University, Kowloon, Hong Kong 999077, People's Republic of China;* orcid.org/0000-0002-6173-5532

Complete contact information is available at: https://pubs.acs.org/10.1021/acs.nanolett.3c03848

Author Contributions

L.Q. carried out the MD simulations. L.Q., W.Y., J.L., Y.W., and X.-S.Y. performed the data analysis. L.Q., Y.W., K.C.C., and X.-S.Y. conceived the storyline of the paper. X.-S.Y. designed and managed the project. All authors contributed to the discussions and wrote the paper. All authors have given approval to the final version of the manuscript.

Notes

The authors declare no competing financial interest.

■ ACKNOWLEDGMENTS

This work was supported by the Hong Kong Research Grants Council (No. 15210123), PolyU grant (No. 1-CD4K), and National Natural Science Foundation of China (No. 51971187). L.Q. and W.Y. were supported by a grant from the Research Committee of PolyU under student account codes RK2U and RK3J, respectively.

■ REFERENCES

(1) Jang, D.; Greer, J. R. Transition from a strong-yet-brittle to a stronger-and-ductile state by size reduction of metallic glasses. *Nat. Mater.* **2010**, *9* (3), 215−219.

(2) Sun, L. G.; Wu, G.; Wang, Q.; Lu, J. Nanostructural metallic materials: Structures and mechanical properties. *Mater. Today* **2020**, *38*, 114−135.

(3) Shang, Z.; Sun, T.; Ding, J.; Richter, N. A.; Heckman, N. M.; White, B. C.; Boyce, B. L.; Hattar, K.; Wang, H.; Zhang, X. Gradient nanostructured steel with superior tensile plasticity. *Sci. Adv.* **2023**, *9* (22), No. eadd9780.

(4) Cao, P. The Strongest Size in Gradient Nanograined Metals. *Nano Lett.* **2020**, *20* (2), 1440−1446.

(5) Meyers, M. A.; Mishra, A.; Benson, D. J. Mechanical properties of nanocrystalline materials. *Prog. Mater. Sci.* **2006**, *51* (4), 427−556.

(6) Dao, M.; Lu, L.; Asaro, R.; Dehosson, J.; Ma, E. Toward a quantitative understanding of mechanical behavior of nanocrystalline metals. *Acta Mater.* **2007**, *55* (12), 4041−4065.

(7) Schiøtz, J.; Jacobsen, K. W. A maximum in the strength of nanocrystalline copper. *Science* **2003**, *301* (5638), 1357−1359.

(8) Hahn, E. N.; Meyers, M. A. Grain-size dependent mechanical behavior of nanocrystalline metals. *Mater. Sci. Eng., A* **2015**, *646*, 101−134.

(9) Chen, W.; You, Z. S.; Tao, N. R.; Jin, Z. H.; Lu, L. Mechanically-induced grain coarsening in gradient nano-grained copper. *Acta Mater.* **2017**, *125*, 255−264.

(10) Tian, L.; Cheng, Y. Q.; Shan, Z. W.; Li, J.; Wang, C. C.; Han, X. D.; Sun, J.; Ma, E. Approaching the ideal elastic limit of metallic glasses. *Nat. Commun.* **2012**, *3*, 609.

(11) Ma, E.; Zhu, T. Towards strength-ductility synergy through the design of heterogeneous nanostructures in metals. *Mater. Today* **2017**, *20* (6), 323−331.
(12) Hasan, M.; Liu, Y.; An, X.; Gu, J.; Song, M.; Cao, Y.; Li, Y.; Zhu, Y.; Liao, X. Simultaneously enhancing strength and ductility of a high-entropy alloy via gradient hierarchical microstructures. *Int. J. Plast.* **2019**, *123*, 178−195.
(13) Wang, J.; Misra, A. Plastic homogeneity in nanoscale heterostructured binary and multicomponent metallic eutectics: An overview. *Curr. Opin. Solid State Mater. Sci.* **2023**, *27* (1), 101055.
(14) Cheng, J. Y.; Xu, S.; Chen, Y.; Li, Z.; Baldwin, J. K.; Beyerlein, I. J.; Mara, N. A. Simultaneous high-strength and deformable nanolaminates with thick biphase interfaces. *Nano Lett.* **2022**, *22* (5), 1897−1904.
(15) Li, B.; Ying, P.; Gao, Y.; Hu, W.; Wang, L.; Zhang, Y.; Zhao, Z.; Yu, D.; He, J.; Chen, J.; et al. Heterogeneous diamond-cBN composites with superb toughness and hardness. *Nano Lett.* **2022**, *22* (12), 4979−4984.
(16) Wu, G.; Chan, K. C.; Zhu, L.; Sun, L.; Lu, J. Dual-phase nanostructuring as a route to high-strength magnesium alloys. *Nature* **2017**, *545* (7652), 80−83.
(17) Katnagallu, S.; Wu, G.; Singh, S. P.; Nandam, S. H.; Xia, W.; Stephenson, L. T.; Gleiter, H.; Schwaiger, R.; Hahn, H.; Herbig, M.; Raabe, D.; Gault, B.; Balachandran, S. Nanoglass-Nanocrystal Composite-a Novel Material Class for Enhanced Strength-Plasticity Synergy. *Small* **2020**, *16* (39), No. e2004400.
(18) Wu, G.; Balachandran, S.; Gault, B.; Xia, W.; Liu, C.; Rao, Z.; Wei, Y.; Liu, S.; Lu, J.; Herbig, M.; Lu, W.; Dehm, G.; Li, Z.; Raabe, D. Crystal-Glass High-Entropy Nanocomposites with Near Theoretical Compressive Strength and Large Deformability. *Adv. Mater.* **2020**, *32* (34), No. e2002619.
(19) Lv, H.; Gao, X.; Zhang, K.; Wen, M.; He, X.; Wu, Z.; Liu, C.; Chen, C.; Zheng, W. Bamboo-like dual-phase nanostructured copper composite strengthened by amorphous boron framework. *Nat. Commun.* **2023**, *14* (1), 4836.
(20) Ming, K.; Zhu, Z.; Zhu, W.; Fang, B.; Wei, B.; Liaw, P. K.; Wei, X.; Wang, J.; Zheng, S. Enhancing strength and ductility via crystalline−amorphous nanoarchitectures in TiZr-based alloys. *Sci. Adv.* **2022**, *8* (10), No. eabm2884.
(21) Wei, B.; Wu, W.; Xie, D.; Nastasi, M.; Wang, J. Strength, plasticity, thermal stability and strain rate sensitivity of nanograined nickel with amorphous ceramic grain boundaries. *Acta Mater.* **2021**, *212*, 116918.
(22) Ding, J.; Neffati, D.; Li, Q.; Su, R.; Li, J.; Xue, S.; Shang, Z.; Zhang, Y.; Wang, H.; Kulkarni, Y.; Zhang, X. Thick grain boundary induced strengthening in nanocrystalline Ni alloy. *Nanoscale* **2019**, *11* (48), 23449−23458.
(23) Wu, G.; Liu, C.; Sun, L.; Wang, Q.; Sun, B.; Han, B.; Kai, J. J.; Luan, J.; Liu, C. T.; Cao, K.; Lu, Y.; Cheng, L.; Lu, J. Hierarchical nanostructured aluminum alloy with ultrahigh strength and large plasticity. *Nat. Commun.* **2019**, *10* (1), 5099.
(24) Wang, Y.; Li, J.; Hamza, A. V.; Barbee, T. W. Ductile crystalline−amorphous nanolaminates. *Proc. Natl Acad. Sci.* **2007**, *104* (27), 11155−11160.
(25) Hua, P.; Xia, M.; Onuki, Y.; Sun, Q. Nanocomposite NiTi shape memory alloy with high strength and fatigue resistance. *Nat. Nanotechnol.* **2021**, *16* (4), 409−413.
(26) Khalajhedayati, A.; Pan, Z.; Rupert, T. J. Manipulating the interfacial structure of nanomaterials to achieve a unique combination of strength and ductility. *Nat. Commun.* **2016**, *7*, 10802.
(27) Hu, X.; Liu, N.; Jambur, V.; Attarian, S.; Su, R.; Zhang, H.; Xi, J.; Luo, H.; Perepezko, J.; Szlufarska, I. Amorphous shear bands in crystalline materials as drivers of plasticity. *Nat. Mater.* **2023**, *22*, 1071.
(28) Guo, W.; Jägle, E.; Yao, J.; Maier, V.; KorteKerzel, S.; Schneider, J. M.; Raabe, D. Intrinsic and extrinsic size effects in the deformation of amorphous CuZr/nanocrystalline Cu nanolaminates. *Acta Mater.* **2014**, *80*, 94−106.
(29) Kim, J.; Jang, D.; Greer, J. R. Nanolaminates Utilizing Size-Dependent Homogeneous Plasticity of Metallic Glasses. *Adv. Funct. Mater.* **2011**, *21* (23), 4550−4554.
(30) Lei, T.; Shin, J.; Gianola, D. S.; Rupert, T. J. Bulk nanocrystalline Al alloys with hierarchical reinforcement structures via grain boundary segregation and complexion formation. *Acta Mater.* **2021**, *221*, 117394.
(31) Pun, S. C.; Wang, W.; Khalajhedayati, A.; Schuler, J. D.; Trelewicz, J. R.; Rupert, T. J. Nanocrystalline Al-Mg with extreme strength due to grain boundary doping. *Mater. Sci. Eng., A* **2017**, *696*, 400−406.
(32) Zhang, P.; Zhang, J. Y.; Li, J.; Liu, G.; Wu, K.; Wang, Y. Q.; Sun, J. Microstructural evolution, mechanical properties and deformation mechanisms of nanocrystalline Cu thin films alloyed with Zr. *Acta Mater.* **2014**, *76*, 221−237.
(33) Luo, J.; Sun, W.; Liang, D.; Yang, W.; Chan, K. C.; Ren, F.; Yang, X. S. An ultra-strong and ductile crystalline−amorphous nanostructured surface layer on TiZrHfTaNb0.2 high-entropy alloy by laser surface processing. *Mater. Des.* **2023**, *227*, 111710.
(34) Sun, W.; Luo, J.; Chan, Y. Y.; Luan, J. H.; Yang, X. S. An extraordinary-performance gradient nanostructured Hadfield manganese steel containing multi-phase nanocrystalline-amorphous core-shell surface layer by laser surface processing. *J. Mater. Sci. Technol.* **2023**, *134*, 209−222.
(35) Hua, P.; Wang, B.; Yu, C.; Han, Y.; Sun, Q. Shear-induced amorphization in nanocrystalline NiTi micropillars under large plastic deformation. *Acta Mater.* **2022**, *241*, 118358.
(36) Wang, B.; Zhang, Z.; Chang, K.; Cui, J.; Rosenkranz, A.; Yu, J.; Lin, C. T.; Chen, G.; Zang, K.; Luo, J.; Jiang, N.; Guo, D. New Deformation-Induced Nanostructure in Silicon. *Nano Lett.* **2018**, *18* (7), 4611−4617.
(37) Wang, H.; Chen, D.; An, X.; Zhang, Y.; Sun, S.; Tian, Y.; Zhang, Z.; Wang, A.; Liu, J.; Song, M.; et al. Deformation-induced crystalline-to-amorphous phase transformation in a CrMnFeCoNi high-entropy alloy. *Sci. Adv.* **2021**, *7* (14), No. eabe3105.
(38) Bai, L.; Wei, B.; Wang, J.; Ming, K.; Zheng, S.; Wang, J. High strength and thermal stability of core-shell Fe-SiOC nanocolumnar composites. *Scr. Mater.* **2022**, *219*, 114885.
(39) Greer, A. L.; Cheng, Y. Q.; Ma, E. Shear bands in metallic glasses. *Mater. Sci. Eng. R Rep.* **2013**, *74* (4), 71−132.
(40) Wang, Y. Q.; Wu, K.; Zhang, J. Y.; Liu, G.; Sun, J. Probing the size- and constituent-mediated mechanical properties and deformation behavior in crystalline/amorphous nanolaminates. *Nanoscale* **2018**, *10* (46), 21827−21841.
(41) Liu, Z. Q.; Liu, G.; Qu, R. T.; Zhang, Z. F.; Wu, S. J.; Zhang, T. Microstructural percolation assisted breakthrough of trade-off between strength and ductility in CuZr-based metallic glass composites. *Sci. Rep.* **2014**, *4*, 4167.
(42) Brink, T.; Albe, K. From metallic glasses to nanocrystals: Molecular dynamics simulations on the crossover from glass-like to grain-boundary-mediated deformation behaviour. *Acta Mater.* **2018**, *156*, 205−214.
(43) Cheng, Z.; Zhou, H.; Lu, Q.; Gao, H.; Lu, L. Extra strengthening and work hardening in gradient nanotwinned metals. *Science* **2018**, *362* (6414), No. eaau1925.
(44) Brandl, C.; Germann, T.; Misra, A. Structure and shear deformation of metallic crystalline−amorphous interfaces. *Acta Mater.* **2013**, *61* (10), 3600−3611.
(45) Zhou, H.; Li, X.; Qu, S.; Yang, W.; Gao, H. A jogged dislocation governed strengthening mechanism in nanotwinned metals. *Nano Lett.* **2014**, *14* (9), 5075−5080.
(46) Gong, H. R.; Kong, L. T.; Lai, W. S.; Liu, B. X. Atomistic modeling of solid-state amorphization in an immiscible Cu-Ta system. *Phys. Rev. B* **2002**, *66* (10), 104204.
(47) Naik, S. N.; Walley, S. M. The Hall-Petch and inverse Hall-Petch relations and the hardness of nanocrystalline metals. *J. Mater. Sci.* **2020**, *55* (7), 2661−2681.
(48) Pan, Z.; Rupert, T. J. Amorphous intergranular films as toughening structural features. *Acta Mater.* **2015**, *89*, 205−214.

https://doi.org/10.1021/acs.nanolett.3c03848
Nano Lett. XXXX, XXX, XXX−XXX

(49) Şopu, D.; Stukowski, A.; Stoica, M.; Scudino, S. Atomic-Level Processes of Shear Band Nucleation in Metallic Glasses. *Phys. Rev. Lett.* **2017**, *119* (19), 195503.
(50) Misra, A.; Hirth, J. P.; Hoagland, R. G. Length-scale-dependent deformation mechanisms in incoherent metallic multilayered composites. *Acta Mater.* **2005**, *53* (18), 4817−4824.
(51) Tian, L.; Wang, X. L.; Shan, Z. W. Mechanical Behavior of Micronanoscaled Metallic Glasses. *Mater. Res. Lett.* **2016**, *4* (2), 63−74.
(52) Wang, C. C.; Ding, J.; Cheng, Y. Q.; Wan, J. C.; Tian, L.; Sun, J.; Shan, Z. W.; Li, J.; Ma, E. Sample size matters for Al88Fe7Gd5 metallic glass: Smaller is stronger. *Acta Mater.* **2012**, *60* (13−14), 5370−5379.

https://doi.org/10.1021/acs.nanolett.3c03848
Nano Lett. XXXX, XXX, XXX−XXX